Supplementary Information

Photogenerated Electron–hole separation–driven CO$_2$ reduction coupled with tetracycline oxidation over LaMnO$_3$ nanoparticles/oxygen–etched g–C$_3$N$_4$ heterojunction: Complementary effects brought by proton transfer

Changye Mang, [a] Xiduan Yang, [a] Jun Luo, *[b] Mingjun Rao, [a] Guanghui Li, *[a] and Tao Jiang [a]

a School of Minerals Processing & Bioengineering, Central South University, Changsha, Hunan 410083, China

b College of Chemistry and Chemical Engineering, Central South University, Changsha Hunan 410083, China

*Corresponding author.
E-mail: liguangh@csu.edu.cn; luojun2013@csu.edu.cn

Experimental Section

Raw materials

La(NO$_3$)$_3$·6H$_2$O (99%), Mn(NO$_3$)$_2$ (50 wt% aqueous solution), citric acid (C$_6$H$_8$O$_7$, ≥99.5%), polyethylene-polypropylene glycol (P123), urea (CO(NH$_2$)$_2$, 99%) NH$_3$·H$_2$O (28 wt%), tetracycline, and ethanol absolute were purchased from Shanghai Macklin Biochemical Co., Ltd. All chemical reagents were analytical grades and used without any further purification.

Characterization techniques

The phase compositions of the samples were determined by an X-ray diffractometer (XRD, D8−Advance, Bruker, Germany). The measurement conditions: b Cu K alpha wavelength of 1.5406 Å, 40 kV voltage, tube current of 30 mA, scanning speed of 10°/min, and scanning range of 5−80°. The morphologies and microstructures of samples were obtained by field emission scanning electron microscopy (FE-SEM, Mira3, Tescan, Czech). The chemical compositions of the samples were characterized by energy dispersive spectrum (EDS). Transmission electron microscopy (TEM), and high-resolution transmission electron microscopy (HRTEM, JEM-2001F JEOL, Japan). Fourier transform infrared (FTIR) spectroscopy spectra were recorded through a KBr pellet technique on an FTIR transmission spectrometer (VERTEX 70, Bruker, Bremen, Germany). X-ray photoelectron spectroscopy (XPS) analysis was conducted on a ESCALAB 250Xi spectrometer (Thermo Fisher Scientific, USA, Al Kα monochromate, hv=1486.6 eV) under a vacuum of $2×10^{-7}$ Pa. Charging effects were corrected by adjusting the main C 1s peak to a position of 284.8 eV. CO_2 adsorption isotherms were collected with an ASAP2460 apparatus (Micromeritics). The samples were degassed in a vacuum at 300°C for 2 h, and then CO_2 adsorption isotherms were measured at 0°C. A chemisorption analyzer (MicrotracBEL BELCAT-B) was used to conduct CO_2 temperature-programmed-desorption (TPD) measurements. The sample was kept at 200 °C for 1 h under an Ar atmosphere, followed by CO_2 adsorption at 50 °C for 0.5 h, and then the desorption of CO_2 was recorded under an Ar atmosphere from 50 to 500°C. Linear sweep voltammetry (LSV) was evaluated in a CO_2-saturated 0.1 M tetraethylammonium bromide acetonitrile solution with and without containing a certain concentration of tetracycline at a scan rate of 0.1 V s $^{-1}$. The UV-vis diffuse reflection spectra (DRS) were obtained for dry-pressed disk samples using a UV-visible spectrophotometer (UV-2550, Shimadzu, Japan). $BaSO_4$ was used as a reflectance standard in the UV-visible diffuse reflectance experiment. The PL spectra were recorded on a fluorescence spectrometer (F-4600, Hitachi). The photoelectrochemical measurements were conducted on CHI 630B workstation; a slurry of the photocatalyst

was spread onto fluorine-doped tin oxide (FTO) glass to prepare the working electrodes. Current-time curves were collected with a 0.1 V bias voltage. The working electrodes were immersed in $NaSO_4$ solution (0.1 M). A saturated Ag/AgCl electrode and a platinum wire were used as the reference electrode and the counter electrode, respectively. Electron spin resonance (ESR) spectroscopy (EMXPLUS, Bruker, Germany) was used to identify reactive oxygen species (ROS) under visible light irradiation, with triethanolamine (TEOA), carbon tetrachloride (CCl_4), 1,4–benzoquinone (BQ) and tert–butyl alcohol (t–BuOH) used to probe the formation of photogenerated holes (h^+), photogenerated electron (e^-), superoxide radicals ($•O^-_2$) and hydroxyl radicals ($•OH$) under aeration. In situ FTIR measurements were carried out with a TENSOR II (Bruker, Germany) spectrometer in the range of 4000–600 cm^{-1}. Then the FTIR spectra were collected in the dark and with irradiation under a CO_2 atmosphere. High-performance liquid chromatography-mass spectrometry (HPLC-MS) were carried out on Nexera-X2UHPLC (Shimadu, Japan) equipped with a photodiode array detector and coupled to the mass spectrometer.

Toxicity analysis method

It was adopted the quantitative structure–activity relationship (QSAR) method to evaluate four index factors: acute toxicity, bioconcentration, development. QSAR method is a statistical analysis approach based on the relationship between the chemical structure of a substance and its biological activity or environmental behavior. The specific model and parameter selection basis of the QSAR method used in this study should be explained as follows: (1) Structure descriptors are used to characterize the structural features of chemical substances, such as molecular size, shape, and charge distribution. (2) Biological activity or environmental behavior indicators are parameters that quantify the effects of chemical substances, such as toxicity, ecotoxicity, and biodegradability. (3) Mathematical models, typically including linear regression and machine learning algorithms, serve as the bridge connecting the two.

Computational details

The structures of $LaMnO_3$, $g–C_3N_4$, $OE–g–C_3N_4$, and $LaMnO_3@OE–g–C_3N_4$ performed using the Vienna Ab-initio Simulation Package (VASP) were applied to design and investigate. The generalized gradient approximation (GGA) in Perdew-Burke-Ernzerhof with Hubbard U corrections (PBE + U) with U value of 3.9 eV and 6.3 eV for Mn and O with the projected augmented wave potentials (PAW) [69] was used as the electron exchange–correlation functional.

In this work, the large convergences of plane electronic wave functions were expanded with the cut-off energy of 450 eV. All the energy of every structure converged to 1×10^{-5} eV, and the force on each atom was less than 0.02 eV $Å^{-1}$. The electronic energies were set to 1×10^{-6} eV in the static self-consistent field (SCF) calculations. The van der Waals (vdW) interaction was used through DFT-D3 correction to obtain a more accurate interaction between CH_4, CO, CO_2, H_2O and as-built structures. 16 Å vacuum spaces were applied to avoid interactions between two layers in nearest-neighbor unit cell. To search the location and minimum energy of transition states for NH_3-SCR were calculated with the climbing-image nudged elastic band method (CI-NEB). Then, the improved dimer method (IDM) was used to refine the structures of the transition state. It was calculated the vibration frequency for each structure of the transition state to confirm only one imaginary frequency is contained. Besides, the Brillouin zone was sampled in a $3 \times 2 \times 2$ Monkhorst-Pack k-point grid.

The adsorption energy (E_{ads}) between gas molecules and substrate is decided by the following formula:

$$E_{ads} = E_{tot} - E_{sub} - E_{adsb} \tag{1}$$

Where E_{tot} is the total energies of the substrate and adsorbate system, E_{sub} is the energies of the substrate and E_{ads} represents the energies of free gas molecules, respectively.

The energy barrier (E_B) of the reaction process is determined by the following equals:

$$E_B = E_{TS} - E_{IM} \tag{3}$$

where E_{IM} is the energy of the intermediate state, and E_{TS} means the transition state in a continuous reaction process.

Photocatalytic experiments

Photocatalytic CO₂ reduction experiment. The performance of photocatalytic CO_2 reduction was performed in Labsolar 6A (Beijing Perfectlight Technology Co., Ltd.) all-glass online closed system. 10 mg of catalyst, 5 mL of acetonitrile (ACN) and 60 mL of deionized water was dispersed in a 100 mL autoclave with a glass window. A 300 W xenon light source (UV-vis IR, PLS-SXE300D, Beijing Perfectlight Technology Co., Ltd. light intensity was 4000 W/m^2) was used to simulate sunlight. After a certain amount of CO_2 was added to the system, the reaction started. The gas products in the reactor were automatically sampled every 0.5 h and injected into gas chromatograph equipped with a flame ionization detector (FID) and a thermal conductivity detector (TCD) (GC9790 II, Zhejiang Fuli Analytical Instrument Co., Ltd.). Finally, the standard curve was used to quantitatively analyze the product.

Photocatalytic degradation experiment. The Photocatalytic experiment of tetracycline was performed in a photoreactor (PL-03, Beijing Precise Technology Co., Ltd., China) equipped with cooling circulating water at 25°C, and a xenon lamp (300 W) worked as light source with an optical filter of $\lambda > 420$ nm and light intensity of about 10.2 mW/cm^2. Tetracycline was selected to be the targeted contaminants to assess the photocatalytic performance of as-synthesized photocatalysts. In detail, 10 mg of photocatalyst was added to 50 mL of targeted solution under magnetic stirring at 600 rpm. Firstly, the suspension was kept for 30 min under a dark environment to reach adsorption equilibrium. After that, the xenon lamp was turned on to trigger the photodegradation reaction. Then, 2 mL of suspensions were periodically collected and filtered using a 0.22 μm syringe filter to remove the photocatalysts. Three parallel results have also been set up in experiment to investigate the repeatability of as-prepared samples.

The concentration of tetracycline was measured by a UV-vis spectrometer at a maximum absorption wavelength of 375 nm. The reaction products were detected by HPLC-MS. The degradation efficiency was fitted using the pseudo-first-order kinetic model. The following equation is displayed:

$$-\ln(C_t/C_0) = kt$$

where C_0 and C_t means the concentration of contaminants at initial stage and time t stage, respectively. k represents the apparent reaction rate constant.

Photocatalytic CO₂ reduction coupled with tetracycline oxidation

A certain amount of tetracycline, 10 mg of photocatalyst, 5 mL of CAN, and 60 mL of deionized water were added in a 100 mL autoclave with a glass window. The other steps are the same as the above steps
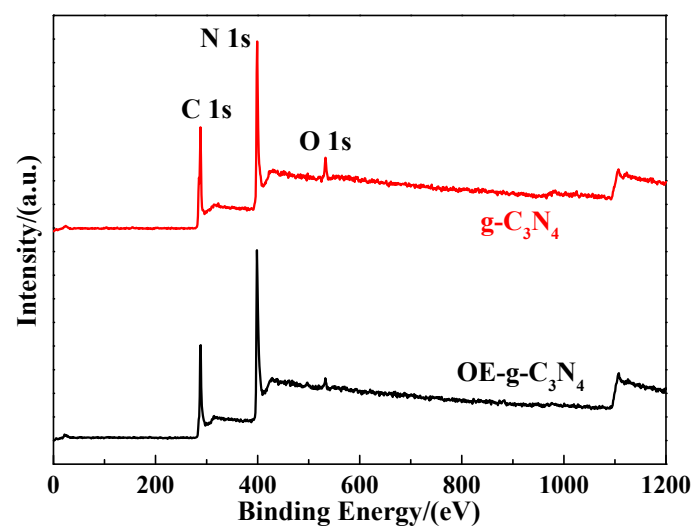
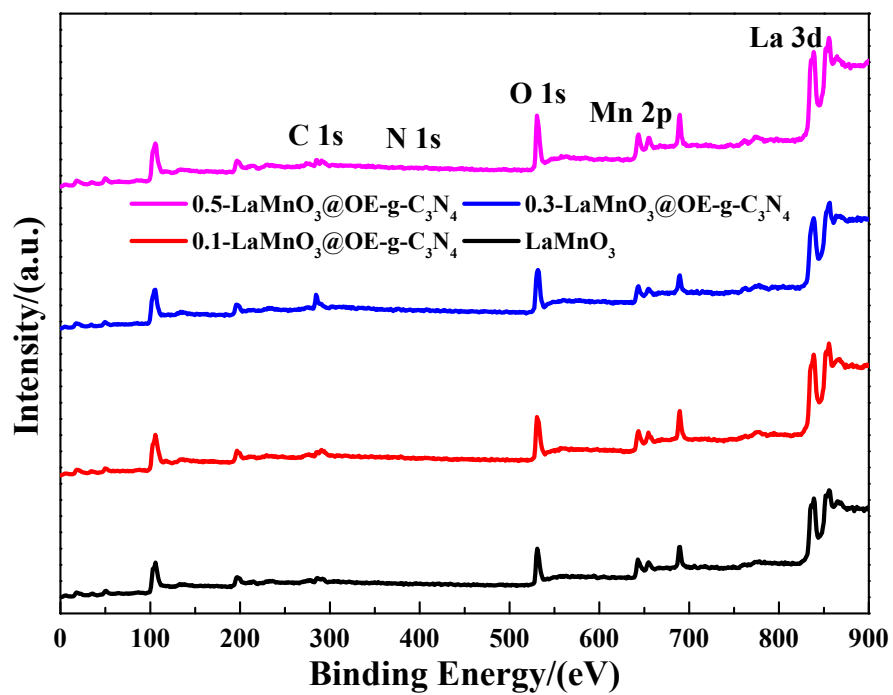Figure S1 XPS full spectra of g-C$_3$N$_4$ and OE-g-C$_3$N$_4$

Figure S2 XPS full spectra of LaMnO$_3$, 0.1-LaMnO$_3$@OE-g-C$_3$N$_4$, 0.3-LaMnO$_3$@OE-g-C$_3$N$_4$, and 0.5-LaMnO$_3$@OE-g-C$_3$N$_4$
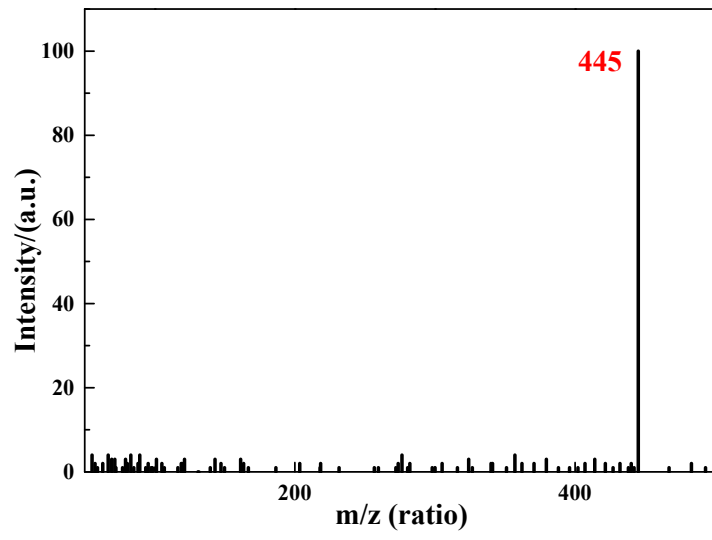
Figure S3 Mass spectra of tetracycline with retention time of 3.95 min
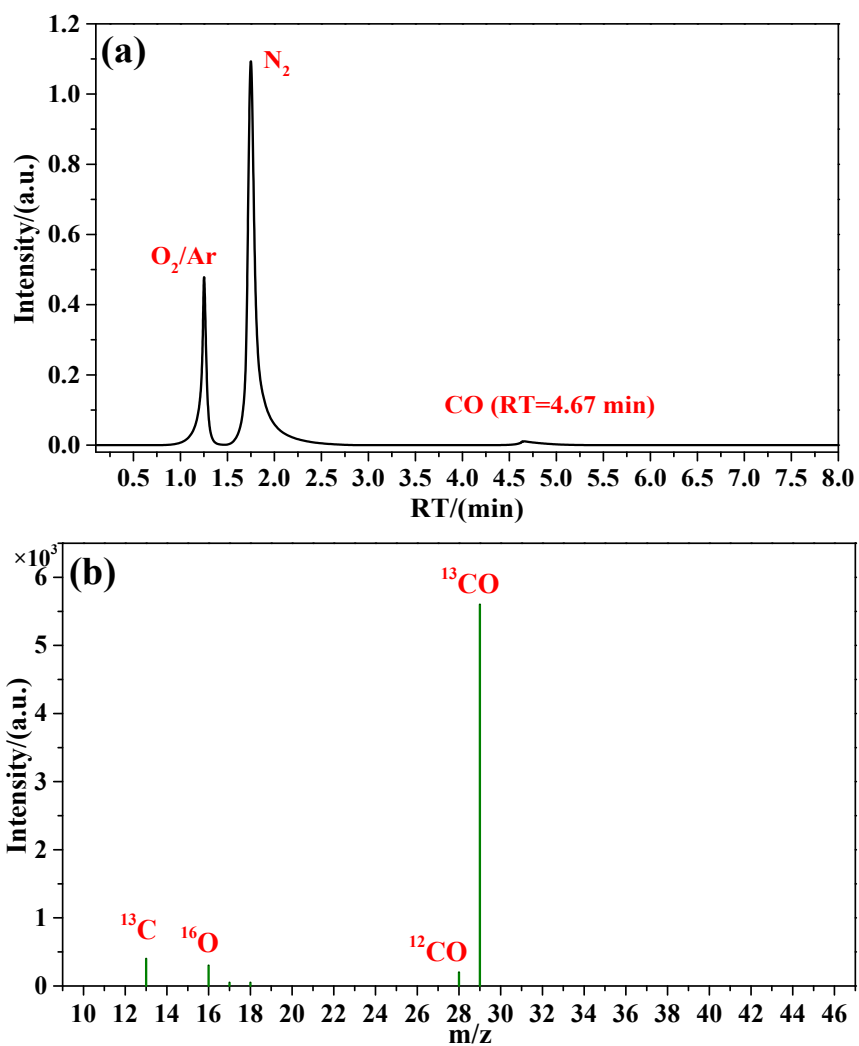
Figure S4 Gas chromatography (a) and mass spectra of ^{13}CO over 0.3–LaMnO$_3$@OE–

g–C$_3$N$_4$ in the photocatalytic reduction of $^{13}CO_2$ under light irradiation for 1 h.

Table S1 The photocatalytic degradation performance of LaMnO$_3$/OE-g-C$_3$N$_4$ heterostructures and other photocatalysts for tetracycline
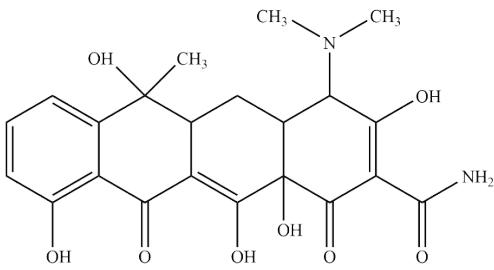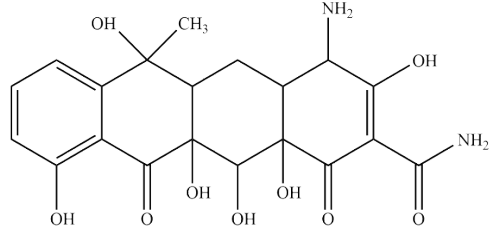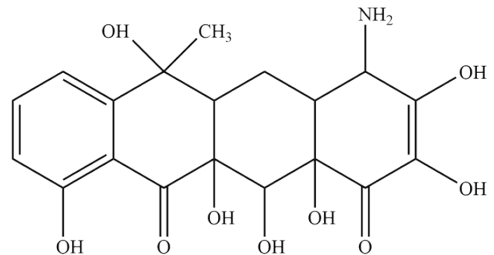
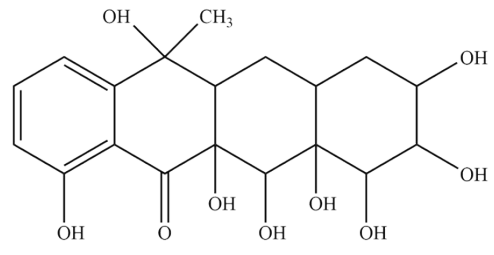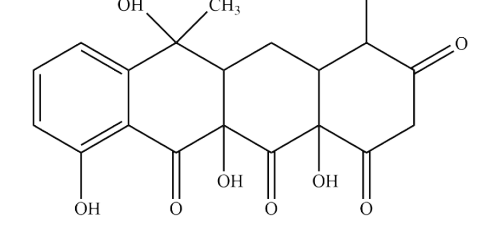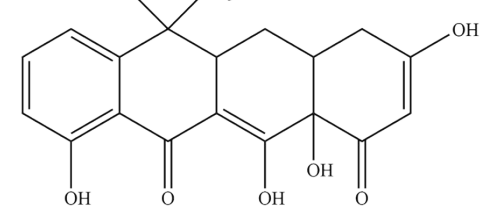| Photocatalyst	Concentration (mg/L)	Dosage (g/L)	Light source	Reaction time (min)	Degradation efficiency	Cost	Stability	Reference
0.3-LaMnO$_3$@OE-g-C$_3$N$_4$	20	0.1	A 300 W Xe lamp, λ≥420 nm	60	100.0%	middle	high	This work
0.1-LaMnO$_3$@OE-g-C$_3$N$_4$	20	0.1	A 300 W Xe lamp, λ≥420 nm	160	100.0%	middle	high	This work
0.5-LaMnO$_3$@OE-g-C$_3$N$_4$	20	0.1	A 300 W Xe lamp, λ≥420 nm	100	100.0%	middle	high	This work
LaMnO$_3$	20	0.1	A 300 W Xe lamp, λ≥420 nm	200	100.0%	middle	middle	This work
g-C$_3$N$_4$	20	0.1	A 300 W Xe lamp, λ≥420 nm	280	100.0%	low	middle	This work
OE-g-C$_3$N$_4$	20	0.1	A 300 W Xe lamp, λ≥420 nm	240	100.0%	low	middle	This work
Sulfur doped carbon quantum dots/hollow tubular g-C$_3$N$_4$	20	1.0	A 300 W Xe lamp, λ≥420 nm	60	82.67%	high	high	[1]
TiO$_2$/Ti$_3$C$_2$T$_x$/AgI	20	2.0	A 500 W Xe lamp, λ≥420 nm	180	97.0%	high	high	[2]
CoP nanoparticles/g-C$_3$N$_4$ nanosheets	10	0.4	A 500 W Xe lamp, λ≥420 nm	120	96.7%	middle	middle	[3]
Ti$_{0.9}$Zr$_{0.05}$Sn$_{0.05}$O$_2$	30	0.8	A 500 W Xe lamp, λ≥420 nm	180	93.0%	middle	high	[4]
g-C$_3$N$_4$ nanoparticles/WO$_3$ hollow microspheres	10	0.4	A 500 W Xe lamp, λ≥420	180	78.4%	middle	middle	[5]

g-C_3N_4@ZIF-8	9	0.5	A 300 W Xe lamp, $\lambda \geq 430$ nm	60	87.6%	middle	high	[6]
g-C_3N_4 decorated ZrO_{2-x} nanotubes	10	0.4	A 300 W Xe lamp, $\lambda \geq 420$ nm	60	90.6%	middle	high	[7]
Bi_2WO_6/polyimide	20	1.0	A 350 W Xe lamp, $\lambda \geq 420$ nm	120	65.1%	middle	high	[8]
MoO_3/Ag/C_3N_4	20	1.0	A 150 W Xe lamp, $\lambda \geq 400$ nm	100	89%	high	middle	[9]
g-C_3N_4/Bi_2WO_6	10	0.5	A 250 W Xe lamp, $\lambda \geq 420$ nm	60	89.1%	middle	middle	[10]

Table S2 Summary of photocatalytic CO_2 reduction to CO

Catalyst	Photosensitizer	Sacrificial agent	Reducing reagent	CO yield (μmol g^{-1} h^{-1})	CO selectivity	Cost	Stability	Reference
0.3–LaMnO$_3$@OE–g–C$_3$N$_4$	None	ACN	tetracycline	538.75	95.25%	middle	high	This work
0.3–LaMnO$_3$@OE–g–C$_3$N$_4$	None	ACN	H$_2$O	113.79	94.32%	middle	high	This work
MAF-34-CoRu	None	None	H$_2$O	11	100.0%	middle	high	[11]
Cu/CN-0.25	None	None	H$_2$O	11	59.3%	low	middle	[12]
Pt/C/CdS@ZnIn$_2$S$_4$/CoO$_x$	None	None	H$_2$O	329	88.6%	high	high	[13]
In@Mo2C-d	None	TEA	H$_2$O	234	97.3%	high	high	[14]
Co-Bi3O4Br-1	None	None	H$_2$O	107.1	99.4%	middle	high	[15]
b-Bi$_2$MoO$_6$	None	None	H$_2$O	8.78	83.22%	middle	high	[16]
Bi$_2$MoO$_6$/BiOI	None	None	H$_2$O	8.34	71.59%	middle	middle	[17]
Bi$_2$MoO$_6$@TiO$_2$	None	None	H$_2$O	30.66	100.0%	middle	middle	[18]
CeO$_2$@In$_2$O$_3$	None	None	H$_2$O	9.65	83.26%	high	high	[19]
Ru/Bi$_2$MoO$_6$	None	None	H$_2$O	23.8	100.0%	high	high	[20]
Au/ZrO$_2$	None	None	TEOA	25.6	83.41%	high	high	[21]

Table S3 Structures of tetracycline and the intermediates in the process of photocatalytic degradation reaction detected with HPLC-MS

Compound	Chemical structure	m/z
Tetracycline (S)		445
S_{B1}		432
S_{B2}		407
S_{B3}		396
S_{C1}		388
S_{A1}		362
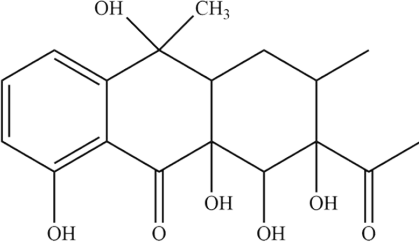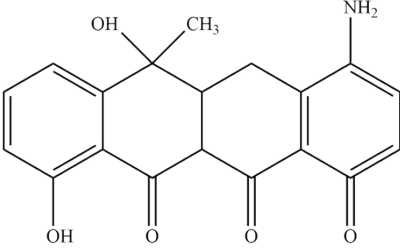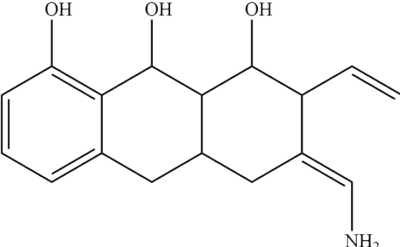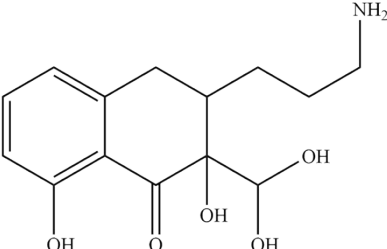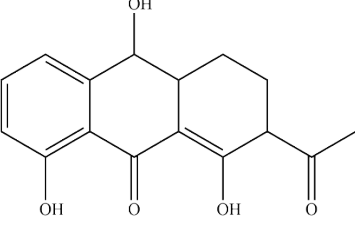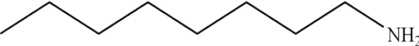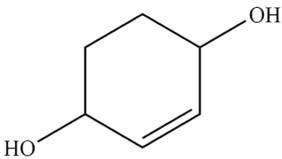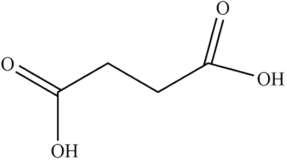
S$_{A2}$		351
S$_{C2}$		340
S$_{B4}$		300
S$_{C3}$		282
S$_{A3}$		274
S$_{B5}$		130
S$_{C4}$		116
S$_{A4}$		118

Table S4 Summary of photocatalytic performance for as-prepared catalysts in this work

Photocatalytic oxidation performance towards TET degradation

Catalyst	TET Removal rate (%)	Time allowance (min)	CO yield ($\mu mol\ g^{-1}\ h^{-1}$)	CH$_4$ yield ($\mu mol\ g^{-1}\ h^{-1}$)
LaMnO$_3$	100	200	-	-
OE–g–C$_3$N$_4$	100	220	-	-
0.1–LaMnO$_3$@OE–g–C$_3$N$_4$	100	160	-	-
0.3–LaMnO$_3$@OE–g–C$_3$N$_4$	100	60	-	-
0.5–LaMnO$_3$@OE–g–C$_3$N$_4$	100	100	-	-

Photocatalytic performance for CO$_2$ reduction reaction

Catalyst	TET Removal rate (%)	Time allowance (min)	CO yield ($\mu mol\ g^{-1}\ h^{-1}$)	CH$_4$ yield ($\mu mol\ g^{-1}\ h^{-1}$)
LaMnO$_3$	-	-	48.61	3.16
OE–g–C$_3$N$_4$	-	-	64.54	8.58
0.1–LaMnO$_3$@OE–g–C$_3$N$_4$	-	-	81.61	2.6
0.3–LaMnO$_3$@OE–g–C$_3$N$_4$	-	-	113.79	6.84
0.5–LaMnO$_3$@OE–g–C$_3$N$_4$	-	-	92.34	6.96

Photocatalytic performance for CO$_2$ reduction coupled with TET oxidation

Catalyst	TET Removal rate (%)	Time allowance (min)	CO yield ($\mu mol\ g^{-1}\ h^{-1}$)	CH$_4$ yield ($\mu mol\ g^{-1}\ h^{-1}$)
LaMnO$_3$	100	120	139.37	8.16
OE–g–C$_3$N$_4$	100	140	281.52	13.58
0.1–LaMnO$_3$@OE–g–C$_3$N$_4$	100	100	426.94	19.72
0.3–LaMnO$_3$@OE–g–C$_3$N$_4$	100	40	538.75	26.84
0.5–LaMnO$_3$@OE–g–C$_3$N$_4$	100	60	484.61	24.96

References:

[1] W. Wang, Z. Zeng, G. Zeng, C. Zhang, R. Xiao, C. Zhou, W. Xiong, Y. Yang, L. Lei, Y. Liu, D. Huang, M. Cheng, Y. Yang, Y. Fu, H. Luo, Y. Zhou, Chem. Eng. J. 378 (2019) 122132.

[2] F.-D. Wu, J.C. Chen, J.P. Hu, J. Environ. Chem. Eng. 10(1) (2022) 107117.

[3] F. Guo, X. Huang, Z. Chen, H. Sun, L. Chen, Chem. Eng. J. 395 (2020) 125118.

[4] H.R. Pouretedal, B. Afshari, Desalin. Water Treat. 57(23) (2016) 10941-10947.

[5] H. Jing, R. Ou, H. Yu, Y. Zhao, Y. Lu, M. Huo, H. Huo, X. Wang, Sep. Purif. Technol. 255 (2021) 117646.

[6] X. Yuan, S. Qu, X. Huang, X. Xue, C. Yuan, S. Wang, L. Wei, P. Cai, Chem. Eng. J. 416 (2021) 129148.

[7] Q. Chen, W. Yang, J. Zhu, L. Fu, D. Li, L. Zhou, J. Hazard. Mater. 384 (2020) 121275.

[8] X. Gao, J. Niu, Y. Wang, Y. Ji, Y. Zhang, J. Hazard. Mater. 403 (2021) 123860.

[9] S. Adhikari, H.H. Lee, D.-H. Kim, Chem. Eng. J. 391 (2020) 123504.

[10] M. Zhang, Y. Zhang, L. Tang, G. Zeng, J. Wang, Y. Zhu, C. Feng, Y. Deng, W. He, J. Colloid. Interf. Sci. 539 (2019) 654-664.

[12] N. Huang, J. Shen, X. Zhang, P. Liao, J. Zhang, and X. Chen, J. Am. Chem. Soc., 2022, 144, 8676-8682.

[13] J. Wang, T. Heil, B. Zhu, C. Tung, J. Yu, H. Chen, M. Antonietti, and S. Cao, ACS Nano, 2020, 14, 8584-8593.

[14] X. Zhang, P. Wang, X. Lv, X. Niu, X. Lin, S. Zhong, D. Wang, H. Lin, J. Chen, and S. Bai, ACS Catal., 2022, 12, 2569-2580.

[15] S. Gong, Y. Niu, X. Teng, X. Liu, M. Xu, C. Xu, T. Meyer, and Z. Chen, Appl. Catal. B Environ., 2022, 310, 121333.

[16] J. Di, C. Chen, S. Yang, S. Chen, M. Duan, J. Xiong, C. Zhu, R. Long, W. Hao, Z. Chi, H. Chen, Y. Weng, J. Xia, L. Song, S. Li, H. Li, and Z. Liu, Nat. Commun., 2019, 10, 2840.

[17] Zhang, Y. Z.; Zhi, X.; Harmer, J. R.; Xu, H. L.; Davey, K.; Ran, J. R.; Qiao, S. Z. Angew. Chem. Int. Ed. 2022, 61, e202212355

[18] Wang, Z. L.; Cheng, B.; Zhang, L. Y.; Yu, J. G.; Li, Y. J.; Wageh, S.; Al-Ghamdi, A. A. Chin. J. Catal. 2022, 43, 1657-1666.

[19] Ren, G. M.; Wei, Z. X.; Li, Z. Z.; Zhang, X. C.; Meng, X. C. Mater. Today Chem. 2023, 27, 101260

[20] Xu, Q. J.; Jiang, J. W.; Wang, X. F.; Duan L. Y.; Guo, H. Rare Met., 2023, 42, 1888-1898.

[21] Ren, G. M.; Liu, S. T.; Li, Z. Z.; Bai, H. C.; Hu, X. D.; Meng, X. C.; Solar RRL. 2022, 6 (7), 2200154.

[22] Gu, M.; Liu, D.; Ding, T.; Liu, X. K.; Chen, T.; Shen, X. Y.; Yao, T. Dalton Trans. 2021, 50, 6076-6082